THE JOURNAL OF PHYSICAL CHEMISTRY B

Article

Ultrafast Time-Resolved Studies on Fluorescein for Recognition Strands Architecture in Amyloid Fibrils

Piotr Hanczyc, Alexander A. Mikhailovsky, David R. Boyer, Michael R. Sawaya, Alan J. Heeger, and David Eisenberg

J. Phys. Chem. B, **Just Accepted Manuscript** • DOI: 10.1021/acs.jpcb.7b07923 • Publication Date (Web): 13 Dec 2017

ACS Publications

The Journal of Physical Chemistry B is published by the American Chemical Society. 1155 Sixteenth Street N.W., Washington, DC 20036

Ultrafast Time-Resolved Studies on Fluorescein for Recognition Strands Architecture in Amyloid Fibrils

Piotr Hanczyc[1*], Alexander Mikhailovsky[2], David R. Boyer[3], Michael R. Sawaya[3], Alan Heeger[1], David Eisenberg[3*]

[1]Center for Polymers & Organic Solids, University of California, Santa Barbara, Santa Barbara, CA 93106, USA

[2]Department of Chemistry & Biochemistry, University of California, Santa Barbara, Santa Barbara, CA 93106, USA

[3]Howard Hughes Medical Institute, UCLA-DOE Institute of Genomics and Proteomics, Los Angeles, California 90095-1570, USA

*correspondence to: david@mbi.ucla.edu ; hanczyc@ucsb.edu

Abstract

Protein aggregation is associated with numerous devastating diseases such as Alzheimer's, Parkinson's, and prion diseases. Development of therapeutics would benefit from knowledge of the structural organization of protein molecules in these amyloid aggregates, particularly in their aqueous biological milieu. However, detailed structural studies to date have been mainly on the solid state, and have required large quantities of purified aggregate. Moreover, these conventional methods require the aggregated assembly to remain structurally stable over days or weeks required to perform the experiment, whereas the pathologically relevant species of in vivo aggregates may be shorter lived. Here, we show the organization of protein chains in dissolved amyloid aggregates can be readily determined spectroscopically using minute quantities of fluorescein-labeled protein segments in a matter of minutes. Specifically, we investigated the possibility of using the ultrafast dynamics of fluorescein to distinguish among three categories of β-sheet geometry: **(1)** anti-parallel in-register, **(2)** parallel in-register or **(3)** anti-parallel out-of-register. Fluorescein, the most commonly used staining dye in biology and medicine, was covalently attached to the N-termini of peptide sequences selected from a library of known amyloid crystal structures. We investigated the aggregates in solution using steady-state and time-resolved absorption and fluorescence spectroscopy. We found that the dynamics of fluorescein relaxation from the excited state revealed amyloid structure-specific information. Particularly, the non-fluorescent cation form of fluorescein showed remarkable sensitivity to local environments created during aggregation. We demonstrate that time-resolved absorption is capable of differentiating strand organization in β-sheet aggregates when strong intermolecular coupling between chromophores occurs. This approach can be useful in optical recognition of specific fibril architectures of amyloid aggregates.

Introduction

Fluorescein belongs to a popular family of xanthene dyes and is widely used in bioresearch[1-2]. Approved by the FDA in 1976, it was accepted in the community as a safe agent for medical applications and treating patients[3]. It was then a natural step forward to explore various biological systems of interest including DNA[4-5], proteins[6-7], or lipid membranes[8] in conjugation with fluorescein. Because of high photoluminescence quantum yield and reproducible photophysical properties it has been used in

imaging[9], cell staining[10], diagnostics[11], eye examination[12], sensing[13], drug delivery[14], and other applications.

However, fluorescein optical properties can be affected by many factors including the pH of dye environment, aggregation, and charge or energy transfer processes that may occur in conjugation with biomolecules[15-17]. In order to get reliable data on fluorescein's behavior in a complex media, such as cellular environment, it is important to know how specific conditions are affecting the optical properties of the dye. The dependence of optical absorption[18], photoluminescence quantum yield[19] (PLQY) and lifetimes[20] of fluorescein dye had been extensively investigated from the middle 70s, but to the best of our knowledge, not the ultrafast transient absorption in the context of dye sensitivity to amyloid polymorphism and strands organization in aggregates associated with neurodegenerative diseases.

Parkinson's, Alzheimer's, and prion diseases are members of a group of over two dozen known amyloid diseases. Amyloid disease patients share in common the deposition of amyloid fibrils detected postmortem in tissues[21]. Amyloid fibrils form when protein molecules aggregate, thereby losing normal biological functions[22]. Mature fibrils from different diseases share common features such as length (>1um), width (8-10 nm), and general architecture of strands oriented perpendicular to the long fibril axis[23]. Furthermore, amyloids, both fibrillar and oligomeric, are composed of β-sheets. However, despite these similarities, a diversity of β-sheet geometries are possible[24], and simulations suggest a diversity of geometries form at the earliest stage of aggregation, called nucleation[25] and morph during the transition to oligomers and fibrils. A rapid and reliable method of interrogation of β-sheet geometry is needed.

Diversity in β-sheet geometry arises from three fundamental levels of organization: (1) the directionality of neighboring β-strands within β-sheets (parallel or antiparallel), (2) the distribution of side chains between the two sheet faces (antifacial or equifacial), and (3) translational shifts of neighboring strands along the strand direction (in-register or out-of-register)[24]. These three levels of organization can appear in any combination, producing at least eight conceivable sheet geometries. Determination of the specific sheet geometry is an emerging challenge for structural biologists, essential to the rational development of therapeutics and novel diagnostics for early detection in amyloid diseases.

We investigated the possibility of using the ultrafast dynamics of fluorescein's excited state to distinguish among three categories of β-sheet geometry: **(1)** anti-parallel in-register, **(2)** parallel in-register or **(3)** anti-parallel out-of-register. The third type of geometry is known to be associated with both amyloid fibrils, and toxic β-barrel-like oligomers[26]. We show that in ultrafast time-resolved absorption experiments, different amyloid architectures create various deactivation channels for the attached chromophores. Peptide sequences from a library of crystallographically determined amyloid fibrils were selected from these three different groups **(1)** GYVLGSA[27], FGAILSS[28]; **(2)** GGNNQQNY[29], LVEALYL[30], NNQNTF[31]; **(3)** ASLTVS, VAVHVF[32]. We monitored changes in dynamics of photogenerated excited states in covalently attached chromophore – fluorescein. Electron microscopy in similar systems showed that chromophore attached to one of the termini can follow peptide self-assembly without disrupting the fibrillization process[33]. In contrast, chromophore photophysics can be affected by

shortening the distance between neighboring dyes upon fibrillization that leads to change of micro-environment, dye aggregation, and intermolecular interactions influencing the relaxation pathway of chromophores[34]. Thus, to investigate fluorescein in different conditions and in conjugation with peptides, we used primarily the time-resolved absorption technique as it shows large sensitivity to conformational changes in peptides and proteins[35-36].

Materials and methods

Fluorescein dye was purchased from Sigma Aldrich and functionalized peptides with fluorescein attached at the N-termini through carboxyl group were purchased from Genscript. All samples were used as obtained. The peptides for optical experiments were dissolved in water buffers and adjusted to a concentration 1 mg/ml, agitated and incubated in elevated temperature at 37C^{o} for 48h. Insoluble aggregates were spun and the exact concentrations were calculated using the molar absorptivity of a fluorescein cation 53 000 M^{-1} cm^{-1} [18]. Fresh made samples were diluted ten times for optical experiments and pH was re-adjusted after checking the absorption spectrum and matching with pristine fluorescein spectrum at the specific pH. The ultrafast transient absorption experiments were first conducted using following peptides **(1)** FGAILSS; **(2)** LVEALYL, NNQNTF; **(3)** VAVHVF. Then a "blind" test was performed and unknown peptides A, B and C were aggregated in the same conditions and recorded dynamics compared with results obtained for structures **(1)**, **(2)** and **(3)**. Proper matching validate described methodology for architecture recognition.

Fibril formation was checked by electron microscopy and β-sheet structure was confirmed by FTIR and diffraction patterns (Fig. S1 and S2).

Drop casted sample on glass slides were tested using Thermo Nicolet iS10 FTIR Spectrometer equipped with Smart Diamond ATR accessory. Working in the mid infrared range of 4,000 to 500 cm^{-1}.

Samples for fiber diffraction and electron microscopy were prepared by the following steps. Peptide stock solutions were diluted to 5 mg/mL in 0.1M phosphate citrate buffer pH 4.0, yielding final buffer concentrations from 70 to 85 mM and total volumes ranging from 128 to 403 µL. Samples were shaken in microcentrifuge tubes for 14 hours at 37° C.

To prepare the fibers for alignment and diffraction, 50 uL of each sample was washed twice to remove any salt that might yield unwanted noise to the background. The washing procedure consisted of centrifuging the samples at 14,000 revolutions per minute at room temperature in a table top centrifuge for 15 min, removing all supernatant, and then resuspending the pellet in 50 µL water. After the second round of washing, the pellet was resuspended in 5 uL of water, and the suspension was pipeted between two glass rods, and allowed to dry at room temperature. Diffraction patterns from the aligned fibers were collected at the Advanced Photon Source, beamline 24-ID-C, using an X-ray wavelength of 0.9202 Å, 100% transmission, 1 s exposure, and 450 mm sample-to-detector distance. The detector was a Pilatus 6M-F pixel detector.

To prepare the samples for electron microscopy, the original fiber concentration was diluted 1:20, and 2 uL were applied to a copper grid (Ted Pella, Inc., 400 mesh, Formvar/Carbon, Product number 01754-F) that had been glow discharged. The samples were stained with uranyl acetate and images collected on a T20 iCorr FEI electron microscope.

Luminescence life-time measurements were performed using Time-Correlated Single Photon Counting (TCSPC) technique[37]. Approximately 100 femtosecond (fs) excitation pulses with wavelength 400 nm were generated by doubling the fundamental frequency of fs Ti:Sapphire laser (Spectraphysics Tsunami) pulses in a commercial optical harmonic generator (Inrad). The laser repetition rate was reduced to 2 MHz by a home-made acousto-optical pulse picker in order to avoid saturation of the chromophore. The TCSPC system is equipped with thermoelectrically-cooled single-photon counting avalanche photodiode (Micro Photon Devices) and electronics board (Becker & Hickl SPC-630) and has instrument response time about 30-40 picoseconds. Triggering signal for the TCSPC board was generated by sending a small fraction of the laser beam onto a fast (400 MHz bandwidth) Si photodiode (Thorlabs Inc.). Fluorescence signal was dispersed in Acton Research SPC-500 monochromator after passing through a pump blocking, long wavelength-pass, autofluorescence-free, interference filter (Omega Filters, ALP series). In addition to the time-resolved detector, the monochromator is equipped with a CCD camera (Princeton Instruments PIXIS-400) allowing for monitoring of the time-averaged fluorescence spectrum. Luminescence transients were not deconvolved with the instrument response function since their characteristic time-constants were much longer than the width of the system response to the excitation pulse.

Transient absorption (TA) measurements were performed using a home-built setup similar to the one described in Ref [38]. The output of a Ti:Sapphire regenerative amplifier (Coherent Astrella, 800 nm, 120 fs, 1.2 mJ pulses with 5 kHz repetition rate) was divided with 10/90 ratio into probe and pump beams, respectively. The probe light was attenuated to μJ level and focused onto 2 mm thick crystalline sapphire plate in [0001] direction to generated supercontinuum. The fs white light was focused onto a sample by a parabolic mirror. The usable spectral range for the supercontinuum probe was 430-750 nm. The pump beam was routed into an optical parametric amplifier (OPA, Light Conversion TOPAS Prime with NirUVis harmonic unit). The OPA output was tuned to 430 nm to match the lowest energy absorption peak in the samples. The pump beam was aligned through a corner cube reflector mounted on a computer-controlled translation stage with 20 cm travel range and 1 μm positioning accuracy (Newport Corp) in order to control the delay between the pump and the probe pulses. The pump and probe beams were focused onto the sample and overlapped spatially at a small angle. A neutral density filter wheel (New Focus Inc) was used to adjust the pump pulse energy. After passing through the sample, the probe beam was dispersed by a Cherny-Turner monochromator (Acton Research SP-300) and detected by a Si photodiode (Oriel) connected to a current preamplifier (SRS SR570). The photodiode signal was then fed into a lock-in amplifier (SRS SR830) synchronized to the first subharmonic of the laser repetition rate (2500 Hz). An optical chopper (New Focus Inc) clocked by the same frequency was used to modulate the pump beam during the differential transmission measurements. A second lock-in amplifier synchronized with the full repetition rate of the laser was used to monitor the probe intensity. The details on the measurement method and chirp correction can be found in the Ref [38]. The instrument response FWHM was measured using non-degenerate two-photon absorption in a crystalline sapphire slide and was found to be about 100 fs with a minor variation at different probe wavelengths.

The samples for TA spectroscopy were placed into quartz cells with optical path length of 1 mm. To avoid observation of pump-dependent effects, such as singlet-singlet annihilation or photochemical

reactions, TA transients were acquired at several, gradually reduced levels of the pump pulse energy until pump-dependent components of the TA signal disappeared.

Dynamics were fitted across the whole decay and analyzed using OriginPro 8.5 software. The data were fitted to a multi-exponential decay of the form:

$$I(t) = A + \sum_{i=1}^{n} B_i e^{-t/\tau_i}$$

Where τ_i is the transient absorption dynamics, B_i is the amplitude of the *i* th decay component, and A is the background noise level. The quality of fits was determined by the reduced chi-squared parameter χ^2.

UV-Vis absorption spectra were collected using Shimadzu UV-2401PC spectrophotometer and PL spectroscopy measurements were conducted on Photon Technology International QuantaMaster fluorimeter.

Results

Steady-state and time-resolved absorption spectroscopy of fluorescein at different pH levels

Fluorescein in solution can exist in a four main prototropic forms – cation, neutral, anion and dianion in the pH range from 2 to 12, and depending on the exact conditions can exist in equilibrated mixture between the several forms that makes the chromophore itself a complex molecule (Fig. 1(a)). Figure 1(b) shows the individual absorption spectra that were extracted by measuring UV-Vis absorption at different pH values. In very acidic (pH<1) and basic (pH>10) environments, the UV-Vis absorption spectra of samples match those of cationic and dianionic species, respectively. For intermediate pH values the spectra of neutral and anionic species can be extracted easily given that at pH=pK_{ai}, where *i* is the index denoting transitions between different ionic states, relative abundances of two prototropic species are equal.

Since each prototropic form has different absorption spectrum and PLQY that in consequence lead to a strong variation in the fluorescein photophysics the UV-Vis absorption spectra of actual samples were measured and shown in Figure 1(c). Most of the experiments with peptides were conducted at pH=2 and in this particular case a shoulder in the absorption spectrum at about 475 nm appears due to the presence of neutral species. The other two tested pH values were pH=7 that is extended towards the blue end of the spectrum compared to that at pH=12 due to the presence of anionic fluorescein. The concentrations of different prototropic species vs pH shown in Figure 1d were calculated based on the pK_a values published in the literature[18].

The reason for such strong differences among ionic species of the chromophore is not fully elucidated, but there is some indication that symmetry of the molecule can be responsible for the optical properties. For example it was shown that the anion form loses symmetry with respect to the dianion and the angle between the plane of xanthene moiety and the plane of the benzoate ring is changed significantly, from 90° to 70° degrees[39]. It leads to distinct changes in spectrum of skeleton vibration modes which can strongly affect the transition moments between different states and consequently influence the optical properties in the ground as well as excited state (Fig. 2). The fact that subtle change in the fluorescein structure can significantly affect its spectral properties makes this chromophore a

promising agent to study β-strand organization in amyloid fibrils where structural differences are in sub-nanometer range. In the case of peptide aggregation, the symmetry of benzoate ring can be strongly affected and fluorescein can act as a sensor of intermolecular interactions when two chromophores appear in a close proximity. We use this advantage to probe fluorescein dynamics that is sterically perturbed by the particular amyloid architecture.

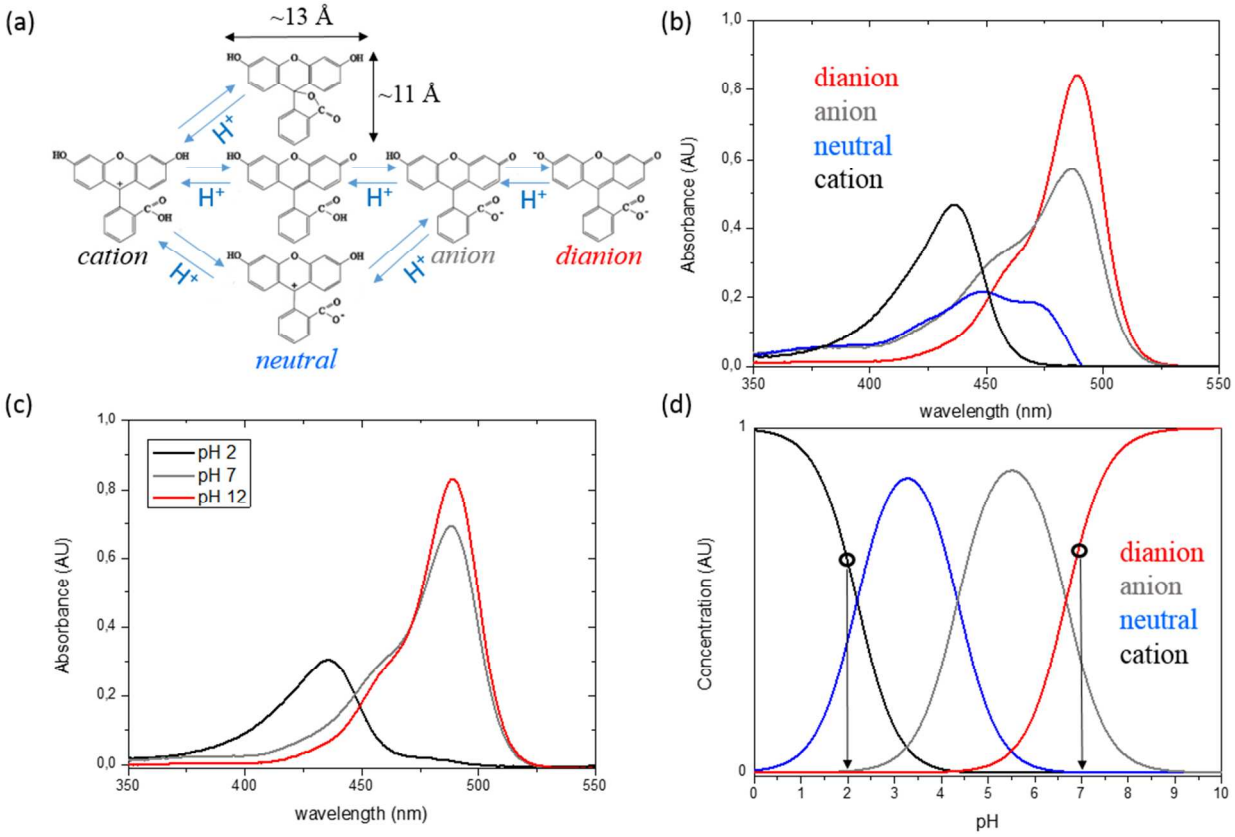

Figure 1 (a) Various pH dependent ionic species of fluorescein and prototropic transition in aqueous solutions; (b) deconvoluted spectra of pure dianion, anion, neutral and cation ionic species; (c) experimental absorption spectra of fluorescein at different pH values; (d) calculated dependence of concentration of different ionic species with marked points representing the pH values at which fluorescein and fluorescein-peptides conjugates were studied (at pH12 a pure dianion is present).

First, careful examination of pristine fluorescein dynamics is required since those data are missing in the literature. This information is required for use as a reference in comparison with amyloid-conjugated fluorescein. Figure 2(a) shows transient absorption spectra of the dye at three different pH levels: pH12, pH7 and pH2 at time delay 1 ps and 50 ps. In case of the dianion form, the ground-state bleaching (GSB) occurs between 450 nm and 520 nm whereas in the region 525-620 nm the stimulated emission (SE) was detected (Fig. S3). A similar case was observed at pH7 where fluorescein exists in a mixture between the anion and dianion form. In pH2 the TA spectrum turns negative around 570 nm indicating that above that wavelength excited state absorption can be detected in acidic conditions. Figure 2(b) represents the dynamics recorded at two wavelengths: 460 nm (GSB) and 530 (SE). The dianion form at pH12 shows linear 5000 ps decay that is similar at both studied wavelengths and reflects the nature of

the dye in basic conditions. At pH7 the three components were resolved: 1.4 ± 0.6 ps, 22 ± 7.1 ps and 4000 ± 500 ps at 460 nm and two components: 2.1 ps and 3500 ± 400 ps at 530 nm. The appearance of shorter-lived components in neutral conditions can be related to anion form that exist in mixture with dianion in pH7. In pH2 the relaxation was as short as 2.85 ± 0.74 ps at both studied wavelengths. It is because the cation form is non-fluorescent and is dominating in acidic environments whereas contributions from other species (e.g. neutral) are below the detection resolution of pump-probe technique. The ultrafast dynamics in pH2 can be attributed to deprotonation of the cation form to amphiprotic water solvent[19]. The process that is responsible for the non-fluorescent nature of the cation form. The long-lived components (>1ns) in neutral and basic conditions can be attributed to fluorescence emission and/or non-radiative relaxation from neutral/anion or dianion forms.

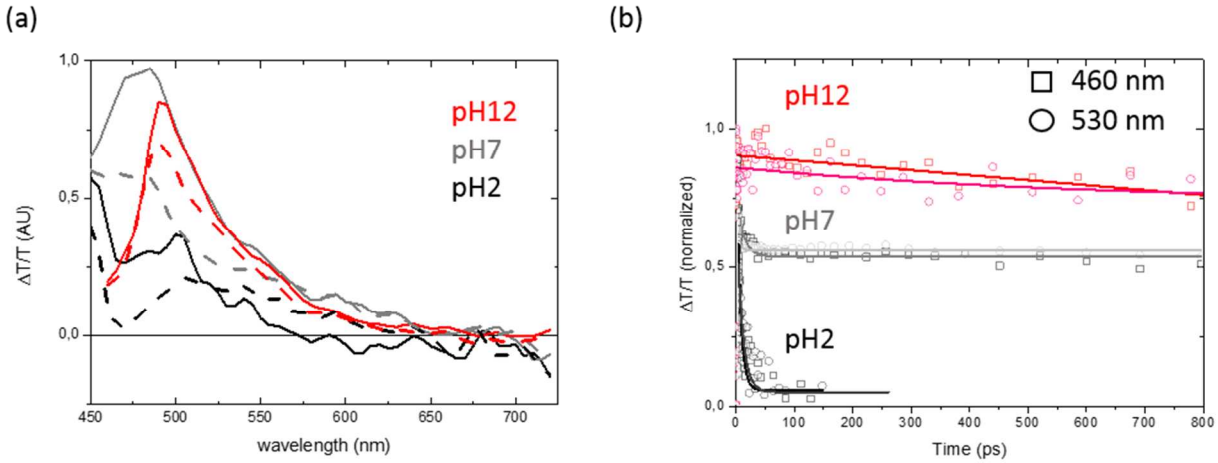

Figure 2 (a) Transient absorption spectra at 1 ps delay (solid lines) and 50 ps delay (dashed lines) and (b) dynamics of fluorescein in different pH conditions: pH12 (red), pH7 (gray) and pH2 (black). The experimental data are presented as either open squares: dynamics at 460 nm or open circles: dynamics recorded at 530 nm.

Fluorescein dynamics in conjugation with peptide in a non-aggregated and aggregated state

In the next step, fluorescein dynamics were analyzed when the molecule was conjugated to the peptide LVEALYL, a segment of the B-chain of insulin. This sequence was chosen because its aggregation can be controlled by pH and there is one tyrosine residue that may affect dye photophysics as was previously suggested[40]. The LVEALYL segment of the protein insulin does not aggregate in basic conditions due to charge repulsion between the glutamic acid (E) residue and its solvent environment (pH12). Adjusting the pH to a level between 6 and 8 causes the formation of morphologically distinct fibrils and acidic conditions at pH below 4 favors formation of mature fibrils[41]. The fibril formation and β-sheet structure in aggregates was confirmed by electron microscopy, FTIR and X-ray diffraction (Fig. S1 and S2). The micrographs indicate also that fluorescein conjugation is not affecting the fibrils morphology.

The dynamics recorded for the fluorescein-LVEALYL conjugate at pH12 at the ground-state bleaching region of 460 nm showed similar behavior to pristine dye (Fig. 3) indicating that amino acid composition and aromatic residues have no influence on fluorescein dynamics when the chromophore is covalently

attached to the N-termini and the peptide remains in a non-aggregated state. Similar results were obtained at stimulated emission region at 530 nm (Fig. S4).

At pH7 a noticeable difference in dynamics of fluorescein was observed when comparing relaxation decays of dye conjugated to the peptide and the pristine chromophore (1.4 ± 0.6 ps, 22 ± 7.1 ps and 4000 ± 500 ps at 460 nm). Three components were resolved at 2.7 ± 0.3 ps, 22 ± 7.1 ps and 3890 ± 200 ps for LVEALYL-fluorescein at pH7. A possible explanation is that some initial aggregates are formed at neutral pH that affect the relaxation of dye molecules. Noteworthy, the signal also rises between 80 and 150 ps. This could be a side effect of the excited state of the fluorescein anion that when attached to the peptide becomes unstable and loses the second proton whereby forming a dianion that has a higher transition moment (TA signal is proportional to the transition moment) and raises the signal in the picosecond time domain.

Likewise the insulin segment, LVEALYL, forms fibrils at pH2 and its crystal structure shows that β-strands are organized in parallel in-register **(2)** β-sheets[30]. The aggregation caused a remarkable change in the fluorescein dynamics when compared to the pristine dye; complex relaxation was revealed with three components 0.19 ± 0.05 ps, 16.9 ± 5.2 ps and 107 ± 22.4 ps (Fig. 3 bottom panel). Particularly interesting is the appearance of a long lived component that may indicate the change in the fluorescein lifetime when the dye aggregates with the peptide. In order to further analyze the effect of aggregation, fluorescein lifetime time-correlated single photon counting (TCSPC) experiments were performed.

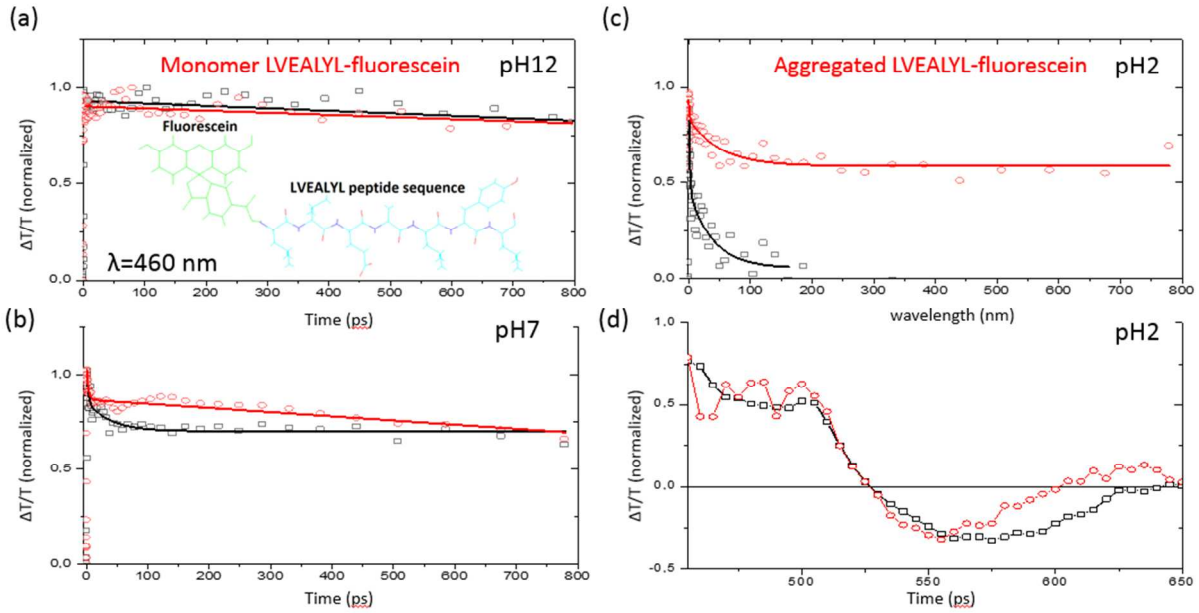

Figure 3 Time-resolved absorption dynamics of pristine fluorescein (black) and fluorescein-LVEALYL conjugates (red) recorded at 460 nm: (a) at pH12 where LVEALYL is in a monomeric state. The inset drawing representing fluorescein-LVEALYL conjugate, (b) dynamics at pH7 where LVEALYL forming intermediate aggregates, (c) dynamics at pH2 where LVEALYL is in an aggregated state, (d) transient absorption spectrum at pH2 (aggregated LVEALYL). Labeled samples concentrations were (a) 4.5 μM. (b) 5.3 μM (c) and (d) 8.4 μM.

Time-resolved fluorescence of fluorescein and fluorescein-peptide aggregates

In order to determine whether peptide aggregation affects the fluorescein photoluminescence emission lifetime and efficiency, we performed steady-state fluorescence and time correlated single photon counting (TCSPC) experiments.

In general, photophysics of xanthene dyes, and fluorescein in particular, has been extensively studied in a monomer and aggregated state[42-44]. Aggregation was usually recognized by red-shifting of the emission spectrum and noticeable changes in the fluorescence lifetime[45].

Since the differences in dynamics of pristine fluorescein and fluorescein conjugation with LVEALYL were most pronounced at pH2, and that such low pH conditions were previously reported to be effective for promoting aggregate self-assembly, we assumed pH2 is an optimal value at which to study the photophysics of other peptide-fluorescein conjugates, making data interpretation feasible. The inset of Figure 4 shows that steady-state emission spectra are red-shifted in conjugates as a consequence of aggregation[46]. The lifetime data of the chromophore alone and in conjugation with peptides representing each β-sheet architecture **(1)**, **(2)** and **(3)** showed a monoexponential decay where fitting revealed a 2 ns component for pristine dye and 2.7 ns for fluorescein in conjugation with aggregated peptides (Fig. 4 and Fig. S5, S6 including explanation and table summarizing lifetime data). Fluorescein lifetime is significantly longer than the picosecond decays measured in pump-probe experiments at pH2. The lifetime is related to resolution and sensitivity whereby TCSPC is capable of detecting the fluorescent species even at very low concentrations; (that is below the detection limit of pump-probe technique). At pH2, a dominating form of fluorescein is a non-fluorescent cation while a small fraction of neutral species that is fluorescent is also present (Fig. 1(b)). Thus, we assume that the photoluminescence emission with 2 ns lifetime is predominantly from the neutral form of fluorescein.

Longer lifetimes in aggregated fluorescein-peptide (compared to pristine fluorescein) can be explained by change of the solvent micro-environment that can particularly affect the cation photophysics[18]. The most plausible mechanism is the restriction of proton transfer to solvent molecules as a consequence of aggregation and solvent reorganization that is manifested with longer lifetimes[47]. The TCSPC results are then in good agreement with pump-probe data where the long lived component was resolved only in the aggregated state thus indicating a change in the deprotonation rate. But all studied zippers showed identical lifetime values indicating that cation form may have some contribution in decay trend but eventually the neutral form is dominating and is similar in each amyloid architecture. Therefore, the TCSPC operating in pico- and nanosecond time domain provide limited access to the cation form, making this particular technique adequate to study amyloid aggregation but uninformative of fibril strand organization that requires a fluorescence up-conversion system for analyzing short-lived states in the femtosecond time regime.

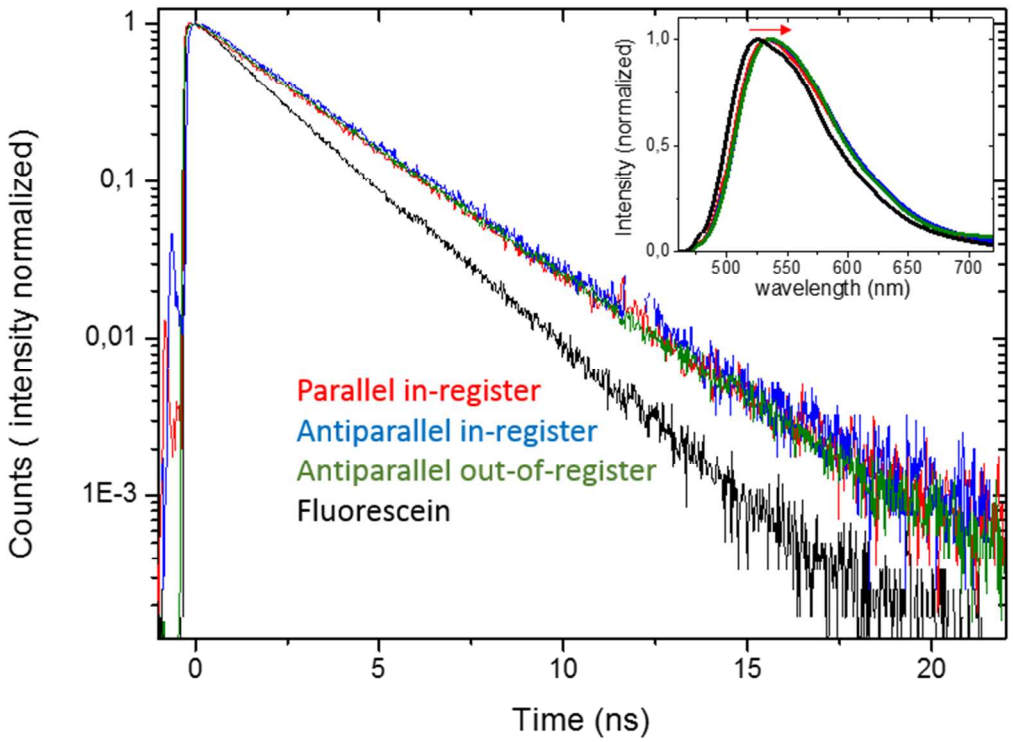

Figure 4 Lifetime data of fluorescein recorded at 530 nm (black) and in conjugation with three different zipper structures ***(1)*** *antiparallel in-register (blue),* ***(2)*** *parallel in-register (red),* ***(3)*** *antiparallel out-of-register (green), all samples measured at pH 2. The inset is the steady-state fluorescence spectra with arrow indicating red-shifting of the spectrum when fluorescein is in conjugation with peptides in the aggregated state. The representative lifetimes are shown for aggregated peptides: FGAILSS, 7.2 µM (1), LVEALYL, 7.5 µM (2) and ASLTVS, 5.4 µM (3) that had no aromatic amino acid in the sequence.*

Transient absorption of fluorescein-peptide aggregates

In order to elucidate whether β-strand organization of fibrils affects the relaxation of the cation form of fluorescein, transient absorption was employed to probe chromophore photophysics in the three sheet geometries **(1)**, **(2)**, **(3)**. The intermolecular distance between fluorescein molecules when it is conjugated with peptides is constrained to be within ångstrom distances whereas the exact separation is determined by the β-sheet organization in the peptide aggregates. In parallel in-register fibrils **(1)** the fluorescein labels are spaced 4.8Å apart whereas in antiparallel in-register **(2)** the spacing is doubled to 9.6Å. In antiparallel out-of-register **(3)** sheet geometry the separation between fluorescein labels is 12Å[48] (Fig. 5(a)). The dimensions of fluorescein molecule (13 Å x 11 Å)[49] is relatively large compared to the separation between the strands and guarantees strong coupling between chromophores[50]. Simultaneously the X-ray data confirms that interspace between β-sheets is not perturbed by fluorescein conjugation (Fig. S2).

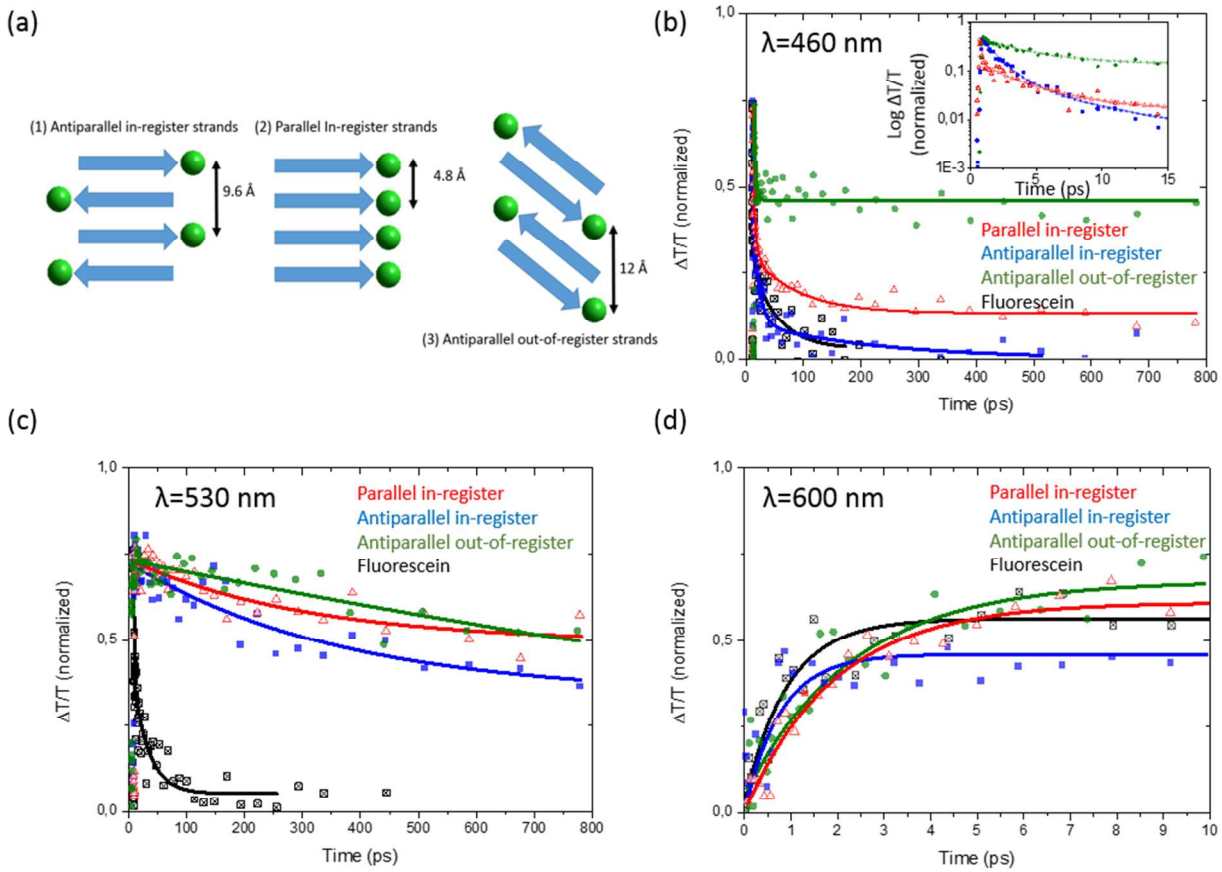

Figure 5 (a) Schematic drawing of strand architectures in the three β-sheet architectures with chromophore attached ***(1)*** *antiparallel in-register,* ***(2)*** *parallel in-register,* ***(3)*** *antiparallel out-of-register. Dynamics of pristine fluorescein (black) and in conjugation with peptides forming different β-sheet architectures (blue,* ***1)*** *, (red,* ***2****), (, green,* ***3****) at (b) 460 nm. The inset of Fig. b represents time domain window >15 ps; (c) dynamics at 530 nm and (d) at 600 nm. Presented dynamics in the graphs are representative decays of fluorescein conjugated with: GYVLGSA, 7.7 μM* ***(1)****; NNQNTF, 8 μM* ***(2)*** *and VAVHVF, 9.1 μM* ***(3)****. Fitting of all aggregated peptides is summarized in table 1.*

The ultrafast time-resolved absorption of fluorescein constrained in three different sheet geometries measured at a particular wavelength can provide information on chromophore-chromophore interactions in the aggregated state, solvent-chromophore interactions upon reorganization of water molecules during aggregation and nuclear motion of bound chromophores (Fig 5 (b), (c), (d)).

In order to investigate dynamics of fluorescein attached to the specific zipper structures as well as pristine fluorescein, three wavelengths were studied: ground-state bleaching at 460 nm and stimulated emission at 530 nm and 600 nm in order to obtain a comprehensive picture of chromophores dynamics in different fibril architectures. Representative dynamics are shown in Figure 5 (b), (c) and (d) and fitting summarized in Table 1 for reference samples **(1)** FGAILSS; **(2)** LVEALYL, NNQNTF; **(3)** VAVHVF and for "blind" test samples GYVLGSA, GGNNQQNY, ASLTVS. Good matching of the fitting curves between reference samples and blind test indicate that transient absorption is providing reproducible results for specific amyloid architectures (Fig. S7). Dynamics of fluorescein conjugated with different peptide

sequences show common features in relaxation decays that can be attributed to chromophores organization in the fibrils.

Unlike in pristine fluorescein where only fast decay (2.84 ps) was recorded at 460 nm, the dynamics in group **(1)** fibrils required fitting with at least two components: 0.94 ± 0.30 ps and 17.3 ± 6.38 ps for GYVLGSA and 0.82 ± 0.32 ps and 23.1 ± 4.83 ps for FGAILSS that is related to change of microenvironment and deprotonation rate due to aggregation of conjugates.
Even more complex relaxation was recorded for parallel in-register fibrils **(2)** NNQNTF and GNNQQNY where three components were resolved: 0.68 ± 0.11 ps, 16.7 ± 4.45 ps and 238 ± 102 (NNQNTF) and 0.18 ± 0.06 ps, 3.35 ± 0.64 ps and 74.8 ± 14.2 ps (GNNQQNY). Comparing to group **(1)** antiparallel in-register fibrils, a longer lived component appeared in group **(2)** indicating rearrangement of covalently attached chromophores that lead to occurrence of emissive states in the fluorescein cation.
The third group is antiparallel out-of-register fibrils **(3)** VAVHVF and ASLTVS that also exhibit a fast decay and a long-lived component; VAVHVF: 1.20 ± 0.12 ps and 340.6 ± 49.5 ps and ASLTVS: 0.24 ± 0.06 and 309.3 ± 71.5 ps, respectively. Also in group (3) the multiexponential decay can be attributed to changes in deportation rates (short-lived components) and conversion of fluorescein cation into emissive species (long-lived component).

Comparing the dynamics of all three fibril groups with that of pristine fluorescein it becomes clear that a strong coupling between chromophores must occur in the processes of aggregation for all samples studied and through-space interactions lead to significant changes in rates required for repopulating the ground-state. Since the differences in fluorescein dynamics can be resolved only in the ultrafast time domain we conclude that cation deprotonation process is most affected, but to a different extent depending on the β-sheet geometry adopted during aggregation.

As a consequence of the change in deprotonation rates, the analysis at stimulated emission region at 530 nm provides the information on solvent-chromophore interactions. The dynamics of three amyloid architectures exhibit one order of magnitude longer decays than the pristine dye and were on average: 360 ps ± 100 ps **(1)**, 320 ps ± 65 ps **(2)** and 710 ps ± 190 ps **(3)**. The results indicate that solvent molecules were reorganized in the hydration shell of aggregates[51] and restriction of proton transfer led to activation of emissive states in the cation form[47]. This observation is consistent with longer fluorescence lifetime data measured at the same wavelength but with the difference that the relaxation decays in pump-probe experiments are amyloid architecture dependent.

Further analysis of dynamics at 600 nm shows peptide structure-dependent rise of signals that can be explained using the Franck-Condon principle. It assumes that electronic transitions in both directions are much faster than nuclear motion, thus they are usually shown as vertical lines on the energy-nuclear coordinate diagram. The dynamics at 600 nm mostly refers to the emissive states that are the resulting products of the nuclear reorganization following the absorption of the photon. In each type of aggregates **(1)**, **(2)** or **(3)**, certain degrees of the nuclear motion may be restricted affecting rate of vibrational relaxation and formation of the state producing the fluorescence.

The dynamics at ultrafast domain was 0.55 ps ± 0.1 ps for pristine dye and was visibly longer in dye conjugated with **(1)** 0.78 ps ± 0.25 ps, **(2)** 3.1 ps ± 0.9 ps, **(3)** 2 ps ± 0.4 ps. The transfer of magnetization between different nuclear spins depends on dipole-dipole (through-space) interactions and surroundings of the sample molecules[52]. The larger is the space between the nuclei, the less efficient is the interaction. Thus, the dynamics measured at 600 nm shows that nuclei of different chromophores interact with each other in a slightly different manner in amyloid architectures.

Table 1. Summary of dynamics at pH2 of fluorescein conjugated with aggregated amyloid segments forming different β- sheet structures and the relative contribution of each component in percent.

Sample	460 nm (GSB) ps	530 nm (SE) ps
Fluorescein at pH2	2.85 ± 0.74	2.84 ± 0.85
Antiparallel in-register **(1)**		
GYVLGSA	0.94 ± 0.30 (65%) 17.3 ± 6.38 (35%)	353 ± 104
FGAILSS	0.82 ± 0.32 (62%) 23.1 ± 4.83 (38%)	375 ± 110
Parallel in-register **(2)**		
LVEALYL	0.19 ± 0.05 (30%) 16.9 ± 5.2 (37%) 107 ± 22.4 (33%)	342 ± 45
NNQNTF	0.68 ± 0.11 (33%) 16.7 ± 4.45 (41%) 238 ± 102 (26%)	314 ± 98
GNNQQNY	0.18 ± 0.06 (32%) 3.35 ± 0.64 (35%) 74.8 ± 14.2 (33%)	321 ± 107
Antiparallel out-of-register **(3)**		
VAVHVF	1.20 ± 0.12 (53%) 340.6 ± 49.5 (47%)	690 ± 230
ASLTVS	0.24 ± 0.06 (51%) 309.3 ± 71.5 (49%)	730 ± 189

Discussion

Unlike electrostatic dyes that were reported to influence the aggregation of protein and peptides[53], the impact of covalently attached chromophores on aggregation was studied to a lesser degree. Existing reports indicate that even large and bulky dyes do not interfere with aggregation and only after long incubation time some morphological changes can be observed[54]. Fluorescein derivatives were previously confirmed to be good candidates to study the proteins and peptides aggregation. Time-resolved and

nonlinear spectroscopy were used in many configurations to analyze the structural organization of modified peptides with dyes[45, 55]. The overall results obtained with applicable methodology for amyloid fibrils structure analysis indicate that fluorescein derivatives do not affect the aggregation even of short peptides. In respect to the existing literature, we suggest that nonlinear and ultrafast spectroscopy can be potentially used to analyze strands organization in amyloid fibrils.

In present case, in order to elaborate on differences in recorded dynamics in amyloid-fluorescein structures we adapt the dimer model developed by Arbeloa *et al.* for the pristine dye[42] and take into consideration that the cation is sensitive to solution organization that depends on amyloid architecture. The pristine dye monomers in free dimer are in parallel planes forming an angle of 76°. In case of amyloid-fluorescein, the fibril architectures **(1)**, **(2)** or **(3)** sterically determine the exact angle between neighboring chromophores. The dynamics then depend both on that angle and the symmetry of the two molecules, where the angle formed by the pair of benzoate rings in respect to the tilted xanthene moieties is most likely responsible for specific relaxation decay.

Also interesting is the relatively long decay time of fluorescein in conjugation with fibrils from group **(2)** and **(3)**. We propose that this length might be related to changes in the hydration shells[56-57] where group **(2)** fluorescein molecules are densely packed (only 4.8Å separations between strands) in a ladder type structure and access of water molecules is limited. Noteworthy, the interspace distance between chromophores in fibrils group **(2)** is nearly identical with the fluorescein dimer where two chromophores are at a distance of 4.6Å[42]. Therefore, a redistribution of solvent molecules must occur around the chromophores as well[58] and the local environment becomes more hydrophobic[59-60] creating new conditions for energy distribution in the ground- and excited state that are considerably different than in the monomer dye or even fibrils from group **(1)** where the interspace is twice as large (9.6 Å) and more access of water is plausible. In line with this hypothesis is the explanation of long decay time in group **(3)** fibrils; in this particular architecture where sheet curvature into barrel-like structures have been observed, the chromophores can be buried inside the barrel which shields the chromophore from solvent molecules. The cation form of fluorescein is particularly vulnerable to changes in solvation environment and cybotactic region whereas reduced access of water molecules to the chromophore significantly decreases the rate of proton transfer from cationic species to water acceptors.

In consequence of different rates of deprotonation, reorganization of solvent molecules in the hydration shells and distance dependent through-space coupling of neighboring fluorescein molecules, the occurrence of different relaxation pathways is highly probable.

In summary, the ability of time-resolved absorption to analyze ground and excited states allows one to collect information on the molecular arrangement of chromophores in the fibril structures. Taking together the three wavelengths 460 nm, 530 nm and 600 nm our work suggests that using the micro-environment sensitive cation form of fluorescein, the time-resolved absorption methodology can be used to differentiate fibril architecture by monitoring chromophore-chromophore interactions and their dynamics. That was confirmed by performing the “blind” test where unknown peptides A, B and C were aggregated and decaying trends compared with dynamics at each wavelength obtained for structures

(1), **(2)** and **(3)**. Proper matching of fitting curves (within the errors due to scattering) validates that chromophores organization in "blind" test samples is the same as in the reference structures.

Conclusions

In this paper we analyze the dynamics of fluorescein in relation to aggregating peptides. Overall results confirm that chromophores organization is determined by the fibrils architecture and that relaxation depends on the rate of intermolecular interactions and solvation shell around the fluorescein-fibrils conjugates. The results indicate that ultrafast time-resolved absorption spectroscopy is capable of following the deprotonation process of the fluorescein cation that can be helpful in resolving structural differences in amyloid fibrils. In this study, the particular emphasis was put on differentiating three amyloid geometries **(1)** antiparallel in-register, **(2)** parallel in-register and **(3)** antiparallel out-of-register. It may be that one of these is preferentially involved in neurodegeneration[61] and this methodology may help to resolve the early stages of its aggregation. Relying on available crystallographic structures, we show that transient absorption can be useful in distinguishing different fibril structures in a solution environment that is closer to physiological conditions than the crystalline state. These results are consistent with the general efforts made on developing tools such as pump-probe microscopy[62] or systems for single molecule detection[63] for investigating structure and dynamics of molecules relaying on the absorption based methods.

Associated Content

Supporting information: (1) FTIR spectra of LVEALAYL in pH12 and pH2, (2) Optical microscope images of aggregated samples, X-ray diffraction patterns and electron micrographs (3) Transient absorption spectra of fluorescein in pH12, (4) Dynamics of pristine fluorescein and fluorescein-LVEALYL peptide at pH12, (5) Wavelength studies of fluorescein lifetimes in conjugation with LVEALYL, (6) Lifetime data of pristine fluorescein (intrinsic and experimental measurements) and fluorescein conjugated with peptides at different pH. Table summarizing the lifetimes. (7) Dynamics fitting of VAVHVF and ASLTVS.

Acknowledgments

P.H. and A. M. thank Dr Dmitry Korystov for supporting data on fluorescein. P.H. acknowledges the support from Swedish Research Council (VR) and International Brain Research Organization (IBRO). A.J.H. thank department of the Navy, Office of Naval Research Award No. N00014-14-1-0580. M.R.S. and D.S.E. thank HHMI and NIH (AG054022) for support. D.R.B is supported by the National Science Foundation Graduate Research Fellowship Program. The ultrafast laser spectroscopy capabilities were supported by DURIP ARO grant 66886LSRIP. This work is based upon research conducted at the Northeastern Collaborative Access Team beamlines, which are funded by the National Institute of General Medical Sciences from the National Institutes of Health (P41 GM103403). The Pilatus 6M detector on 24-ID-C beam line is funded by a NIH-ORIP HEI grant (S10 RR029205). This research used resources of the Advanced Photon Source, a U.S. Department of Energy (DOE) Office of Science User

Facility operated for the DOE Office of Science by Argonne National Laboratory under Contract No. DE-AC02-06CH11357.

References

1. Gurr, E., *Synthetic dyes in biology, medicine and chemistry*. Elsevier: 2012.
2. Vennerstrom, J. L.; Makler, M. T.; Angerhofer, C. K.; Williams, J. A., Antimalarial dyes revisited: xanthenes, azines, oxazines, and thiazines. *Antimicrob. Ag. Chemoth.* **1995,** *39*, 2671-2677.
3. Alford, R.; Simpson, H. M.; Duberman, J.; Hill, G. C.; Ogawa, M.; Regino, C.; Kobayashi, H.; Choyke, P. L., Toxicity of organic fluorophores used in molecular imaging: literature review. *Mol. imag.* **2009,** *8*, 341-354.
4. Wang, S.; Gaylord, B. S.; Bazan, G. C., Fluorescein provides a resonance gate for FRET from conjugated polymers to DNA intercalated dyes. *J. Am. Chem. Soc.* **2004,** *126*, 5446-5451.
5. Telser, J.; Cruickshank, K. A.; Morrison, L. E.; Netzel, T. L., Synthesis and characterization of DNA oligomers and duplexes containing covalently attached molecular labels: comparison of biotin, fluorescein, and pyrene labels by thermodynamic and optical spectroscopic measurements. *J. Am. Chem. Soc.* **1989,** *111*, 6966-6976.
6. Klatzo, I.; Miquel, J.; Otenasek, R., The application of fluorescein labeled serum proteins (FLSP) to the study of vascular permeability in the brain. *Acta Neuropat.* **1962,** *2*, 144-160.
7. Keppler, A.; Gendreizig, S.; Gronemeyer, T.; Pick, H.; Vogel, H.; Johnsson, K., A general method for the covalent labeling of fusion proteins with small molecules in vivo. *Nat. biotech.* **2003,** *21*, 86-89.
8. Berginc, K.; Žakelj, S.; Levstik, L.; Uršič, D.; Kristl, A., Fluorescein transport properties across artificial lipid membranes, Caco-2 cell monolayers and rat jejunum. *Eur. J. Pharm. Biopharm.* **2007,** *66*, 281-285.
9. Giloh, H.; Sedat, J. W., Fluorescence microscopy: reduced photobleaching of rhodamine and fluorescein protein conjugates by n-propyl gallate. *Sci.* **1982,** *217*, 1252-1255.
10. Widholm, J. M., The use of fluorescein diacetate and phenosafranine for determining viability of cultured plant cells. *Stain Technol.* **1972,** *47*, 189-194.
11. Barta, L.; Brooser, G.; Molnár, M., Diagnostic importance of fluorescein angiography in infantile diabetes. *Acta Diabetol. Lat.* **1972,** *9*, 290-298.
12. Korb, D. R.; Greiner, J. V.; Herman, J., Comparison of fluorescein break-up time measurement reproducibility using standard fluorescein strips versus the Dry Eye Test (DET) method. *Cornea* **2001,** *20*, 811-815.
13. Whitaker, J. E.; Haugland, R. P.; Prendergast, F. G., Spectral and photophysical studies of benzo [c] xanthene dyes: dual emission pH sensors. *Anal. Biochem.* **1991,** *194*, 330-344.
14. Combes, R.; Haveland-Smith, R., A review of the genotoxicity of food, drug and cosmetic colours and other azo, triphenylmethane and xanthene dyes. *Mutat. Res. Rev. Gen. tox.* **1982,** *98*, 101-243.
15. Valdes-Aguilera, O.; Neckers, D., Aggregation phenomena in xanthene dyes. *Ac. Chem. Res.* **1989,** *22*, 171-177.
16. Wu, M. M.; Llopis, J.; Adams, S.; McCaffery, J. M.; Kulomaa, M. S.; Machen, T. E.; Moore, H.-P. H.; Tsien, R. Y., Organelle pH studies using targeted avidin and fluorescein–biotin. *Chem. Biol.* **2000,** *7*, 197-209.
17. Ramakrishna, G.; Ghosh, H. N., Emission from the charge transfer state of xanthene dye-sensitized TiO2 nanoparticles: A new approach to determining back electron transfer rate and verifying the marcus inverted regime. *J. Phys. Chem. B* **2001,** *105*, 7000-7008.
18. Sjöback, R.; Nygren, J.; Kubista, M., Absorption and fluorescence properties of fluorescein. *Spectrochim. Acta Mol. Biomol. Spectrosc.* **1995,** *51*, L7-L21.

19. Martin, M. M.; Lindqvist, L., The pH dependence of fluorescein fluorescence. *J. Luminesc.* **1975,** *10*, 381-390.
20. Hammer, M.; Schweitzer, D.; Richter, S.; Königsdörffer, E., Sodium fluorescein as a retinal pH indicator? *Physiol. measur.* **2005,** *26*, 9-12.
21. Tipping, K. W.; van Oosten-Hawle, P.; Hewitt, E. W.; Radford, S. E., Amyloid fibres: inert end-stage aggregates or key players in disease? *Tren. Biochem. Sci.* **2015,** *40*, 719-727.
22. Brettschneider, J.; Del Tredici, K.; Lee, V. M.-Y.; Trojanowski, J. Q., Spreading of pathology in neurodegenerative diseases: a focus on human studies. *Nat. Rev. Neurosci.* **2015,** *16*, 109-120.
23. Makin, O. S.; Serpell, L. C., Structures for amyloid fibrils. *Febs Journal* **2005,** *272*, 5950-5961.
24. Eisenberg, D. S.; Sawaya, M. R., Structural studies of amyloid proteins at the molecular level. *An. Rev. Biochem.* **2017,** *86*, 69-95.
25. Zhang, J.; Muthukumar, M., Simulations of nucleation and elongation of amyloid fibrils. *J. Chem. Phys.* **2009,** *130*, 035102.
26. Laganowsky, A.; Liu, C.; Sawaya, M. R.; Whitelegge, J. P.; Park, J.; Zhao, M.; Pensalfini, A.; Soriaga, A. B.; Landau, M.; Teng, P. K., Atomic view of a toxic amyloid small oligomer. *Sci.* **2012,** *335*, 1228-1231.
27. Yu, L.; Lee, S.-J.; Yee, V. C., Crystal structures of polymorphic prion protein β1 peptides reveal variable steric zipper conformations. *Biochem.* **2015,** *54*, 3640-3648.
28. Soriaga, A. B.; Sangwan, S.; Macdonald, R.; Sawaya, M. R.; Eisenberg, D., Crystal structures of IAPP amyloidogenic segments reveal a novel packing motif of out-of-register beta sheets. *J. Phys. Chem. B* **2015,** *120*, 5810–5816.
29. Nelson, R.; Sawaya, M. R.; Balbirnie, M.; Madsen, A. Ø.; Riekel, C.; Grothe, R.; Eisenberg, D., Structure of the cross-β spine of amyloid-like fibrils. *Nat.* **2005,** *435*, 773-778.
30. Ivanova, M. I.; Sievers, S. A.; Sawaya, M. R.; Wall, J. S.; Eisenberg, D., Molecular basis for insulin fibril assembly. *Proc. Natl. Acad. Sci.* **2009,** *106*, 18990-18995.
31. Wiltzius, J. J.; Landau, M.; Nelson, R.; Sawaya, M. R.; Apostol, M. I.; Goldschmidt, L.; Soriaga, A. B.; Cascio, D.; Rajashankar, K.; Eisenberg, D., Molecular mechanisms for protein-encoded inheritance. *Nat. Struct.. Mol. Bio.* **2009,** *16*, 973-978.
32. Saelices, L.; Johnson, L. M.; Liang, W. Y.; Sawaya, M. R.; Cascio, D.; Ruchala, P.; Whitelegge, J.; Jiang, L.; Riek, R.; Eisenberg, D. S., Uncovering the mechanism of aggregation of human transthyretin. *J. Biol. Chem.* **2015,** *290*, 28932-28943.
33. MacPhee, C. E.; Dobson, C. M., Formation of mixed fibrils demonstrates the generic nature and potential utility of amyloid nanostructures. *J. Am. Chem. Soc.* **2000,** *122*, 12707-12713.
34. Channon, K. J.; Devlin, G. L.; Magennis, S. W.; Finlayson, C. E.; Tickler, A. K.; Silva, C.; MacPhee, C. E., Modification of fluorophore photophysics through peptide-driven self-assembly. *J. Am. Chem. Soc.* **2008,** *130*, 5487-5491.
35. Spörlein, S.; Carstens, H.; Satzger, H.; Renner, C.; Behrendt, R.; Moroder, L.; Tavan, P.; Zinth, W.; Wachtveitl, J., Ultrafast spectroscopy reveals subnanosecond peptide conformational dynamics and validates molecular dynamics simulation. *Proc. Natl. Acad. Sci.* **2002,** *99*, 7998-8002.
36. Chattoraj, M.; King, B. A.; Bublitz, G. U.; Boxer, S. G., Ultra-fast excited state dynamics in green fluorescent protein: multiple states and proton transfer. *Proc. Natl. Acad. Sci.* **1996,** *93*, 8362-8367.
37. Becker, W., *Advanced time-correlated single photon counting techniques*. Springer Science & Business Media: 2005; Vol. 81.
38. Klimov, V. I.; McBranch, D. W., Femtosecond high-sensitivity, chirp-free transient absorption spectroscopy using kilohertz lasers. *Opt. Lett.* **1998,** *23*, 277-279.
39. Wang, L.; Roitberg, A.; Meuse, C.; Gaigalas, A., Raman and FTIR spectroscopies of fluorescein in solutions. *Spectrochim. Acta Mol. Biomol. Spectrosc.* **2001,** *57*, 1781-1791.

40. Blackman, M. J.; Corrie, J. E.; Croney, J. C.; Kelly, G.; Eccleston, J. F.; Jameson, D. M., Structural and biochemical characterization of a fluorogenic rhodamine-labeled malarial protease substrate. *Biochem.* **2002,** *41*, 12244-12252.
41. Shammas, S. L.; Knowles, T. P.; Baldwin, A. J.; MacPhee, C. E.; Welland, M. E.; Dobson, C. M.; Devlin, G. L., Perturbation of the stability of amyloid fibrils through alteration of electrostatic interactions. *Biophys. J.* **2011,** *100*, 2783-2791.
42. Arbeloa, I. L., Dimeric and trimeric states of the fluorescein dianion. Part 1.—Molecular structures. *J. Chem. Soc. Faraday Trans.* **1981,** *77*, 1725-1733.
43. Hennig, A.; Hatami, S.; Spieles, M.; Resch-Genger, U., Excitation energy migration and trapping on the surface of fluorescent poly (acrylic acid)-grafted polymer particles. *Photchem. Photobio. Sci.* **2013,** *12*, 729-737.
44. Nasr, C.; Liu, D.; Hotchandani, S.; Kamat, P. V., Dye-capped semiconductor nanoclusters. Excited state and photosensitization aspects of rhodamine 6G H-aggregates bound to SiO2 and SnO2 colloids. *J. Phys. Chem.* **1996,** *100*, 11054-11061.
45. Esbjörner, E. K.; Chan, F.; Rees, E.; Erdelyi, M.; Luheshi, L. M.; Bertoncini, C. W.; Kaminski, C. F.; Dobson, C. M.; Schierle, G. S. K., Direct observations of amyloid β self-assembly in live cells provide insights into differences in the kinetics of Aβ (1–40) and Aβ (1–42) aggregation. *Chemi. Biol.* **2014,** *21*, 732-742.
46. Martínez Martínez, V.; López Arbeloa, F.; Bañuelos Prieto, J.; López Arbeloa, I., Characterization of rhodamine 6G aggregates intercalated in solid thin films of laponite clay. 2 Fluorescence spectroscopy. *J. Phys. Chem. B* **2005,** *109*, 7443-7450.
47. Ali, M.; Kumar, V.; Pandey, S., Unusual fluorescein prototropism within aqueous acidic 1-butyl-3-methylimidazolium tetrafluoroborate solution. *Chem. Comm.* **2010,** *46*, 5112-5114.
48. Jiang, L.; Liu, C.; Leibly, D.; Landau, M.; Zhao, M.; Hughes, M. P.; Eisenberg, D. S., Structure-based discovery of fiber-binding compounds that reduce the cytotoxicity of amyloid beta. *Elife* **2013,** *2*, e00857.
49. Bain, A.; Chandna, P.; Butcher, G.; Bryant, J., Picosecond polarized fluorescence studies of anisotropic fluid media. II. Experimental studies of molecular order and motion in jet aligned rhodamine 6G and resorufin solutions. *J. Chem. Phys.* **2000,** *112*, 10435-10449.
50. Nenov, A.; Rivalta, I.; Cerullo, G.; Mukamel, S.; Garavelli, M., Disentangling peptide configurations via two-dimensional electronic spectroscopy: ab initio simulations beyond the Frenkel Exciton Hamiltonian. *J. Phys. Chem. Lett.* **2014,** *5*, 767-771.
51. Ravikumar, K. M.; Hwang, W., Role of hydration force in the self-assembly of collagens and amyloid steric zipper filaments. *J. Am. Chem. Soc.* **2011,** *133*, 11766-11773.
52. Chai, M.; Holley, A. K.; Kruskamp, M., Encapsulating fluorescein using adipic acid self-assembly on the surface of PPI-3 dendrimer. *Chem. Comm.* **2007**, 168-170.
53. Groenning, M., Binding mode of thioflavin T and other molecular probes in the context of amyloid fibrils—current status. *J. Chem. Biol.* **2010,** *3*, 1-18.
54. Channon, K. J.; Devlin, G. L.; MacPhee, C. E., Efficient energy transfer within self-assembling peptide fibers: a route to light-harvesting nanomaterials. *J. Am. Chem. Soc.* **2009,** *131*, 12520-12521.
55. Wang, Y.; Clark, T. B.; Goodson III, T., Two-photon and time-resolved fluorescence conformational studies of aggregation in amyloid peptides. *J. Phys. Chem. B* **2010,** *114*, 7112-7120.
56. Massi, F.; Straub, J. E., Structural and dynamical analysis of the hydration of the Alzheimer's β-amyloid peptide. *J. Comp. Chem.* **2003,** *24*, 143-153.
57. Fichou, Y.; Schirò, G.; Gallat, F.-X.; Laguri, C.; Moulin, M.; Combet, J.; Zamponi, M.; Härtlein, M.; Picart, C.; Mossou, E., Hydration water mobility is enhanced around tau amyloid fibers. *Proc. Natl. Acad. Sci.* **2015,** *112* (20), 6365-6370.

58. Klonis, N.; Clayton, A. H.; Voss, E. W.; Sawyer, W. H., Spectral properties of fluorescein in solvent-water mixtures: applications as a probe of hydrogen bonding environments in biological systems. *Photochem. photobio.* **1998,** *67*, 500-510.
59. Lakowicz, J. R.; Keating-Nakamoto, S., Red-edge excitation of fluorescence and dynamic properties of proteins and membranes. *Biochem.* **1984,** *23*, 3013-3021.
60. Chong, S. H.; Ham, S., Interaction with the surrounding water plays a key role in determining the aggregation propensity of proteins. *Angew. Chem. Int. Ed.* **2014,** *53*, 3961-3964.
61. Liu, C.; Zhao, M.; Jiang, L.; Cheng, P.-N.; Park, J.; Sawaya, M. R.; Pensalfini, A.; Gou, D.; Berk, A. J.; Glabe, C. G., Out-of-register β-sheets suggest a pathway to toxic amyloid aggregates. *Proc. Natl. Acad. Sci.* **2012,** *109*, 20913-20918.
62. Fischer, M. C.; Wilson, J. W.; Robles, F. E.; Warren, W. S., Pump-probe microscopy. *Rev. Sci. Instr.* **2016,** *87*, 031101.
63. Arroyo, J. O.; Kukura, P., Non-fluorescent schemes for single-molecule detection, imaging and spectroscopy. *Nat. Phot.* **2016,** *10*, 11-17.

TOC Graphic